

LETTER

Importance of resistivity on edge-localized mode onset in spherical tokamaks

To cite this article: A. Kleiner *et al* 2021 *Nucl. Fusion* **61** 064002

View the [article online](#) for updates and enhancements.

You may also like

- [Machine learning assisted hybrid models can improve streamflow simulation in diverse catchments across the conterminous US](#)
Goutam Konapala, Shih-Chieh Kao, Scott L Painter et al.
- [Impact of shape on pedestal characteristics in the wide pedestal quiescent H-mode in the DIII-D tokamak](#)
T.M. Wilks, L.A. Morton, D.M. Kriete et al.
- [Peeling-ballooning stability of tokamak plasmas with applied 3D magnetic fields](#)
M.S. Anastopoulos Tzanis, C.J. Ham, Snyder P.B. et al.



**IOP | ebooks™**

Bringing together innovative digital publishing with leading authors from the global scientific community.

Start exploring the collection—download the first chapter of every title for free.

Letter

Importance of resistivity on edge-localized mode onset in spherical tokamaks

A. Kleiner^{1,*} , N.M. Ferraro¹, A. Diallo¹  and G.P. Canal²¹ Princeton Plasma Physics Laboratory, PO Box 451, Princeton, NJ 08543-0451, United States of America² Instituto de Física, Universidade de São Paulo, São Paulo, CEP 05508-090, BrazilE-mail: akleiner@pppl.gov

Received 27 January 2021, revised 10 March 2021

Accepted for publication 31 March 2021

Published 28 April 2021

**Abstract**

We explore the impact of realistic plasma resistivity on the linear stability of peeling-ballooning (PB) modes in tokamak discharges with low-aspect ratio. For this study we consider discharges that are subject to edge-localized modes (ELMs) in the National Spherical Torus Experiment (NSTX). Employing the state of the art extended-magnetohydrodynamic (MHD) code M3D-C1 it is demonstrated that non-ideal effects can significantly affect PB stability thresholds in NSTX discharges. In particular, robust resistive PB modes are found to exist well before the ideal PB stability threshold is met. These novel results can explain why ideal-MHD theory often does not accurately describe ELM onset in spherical torus configurations, and also present a valuable basis for the development of a predictive model for ELMs in low-aspect ratio tokamaks.

Keywords: magnetohydrodynamics, NSTX, peeling-ballooning, edge localized modes, pedestal, spherical tokamak

(Some figures may appear in colour only in the online journal)

Spherical tokamaks (STs), i.e. tokamaks with low-aspect ratio [1, 2] are promising candidates for economically viable fusion reactors due to their smaller size, higher normalized pressure, and higher bootstrap current [3] fraction. A particular advantage of STs is improved (ideal) magnetohydrodynamic (MHD) stability [4–6]. Periodic relaxations of the edge pressure gradient along with expulsion of particles and heat have been observed in spherical and conventional aspect ratio tokamaks operating in the high-confinement mode (H-mode) [7]. These instabilities, called edge-localized modes (ELMs) [8], limit the performance of present day machines and are a major issue for reactor scale tokamaks due to large heat loads to plasma facing components [9]. The peeling-ballooning (PB) model [10] provides an understanding of ELMs in terms of macroscopic MHD instabilities, where ballooning modes (having high toroidal mode number n) are driven by the large pres-

sure gradient and peeling modes (low- n) by the current density at the edge transport barrier (commonly referred to as pedestal) [11, 12]. The onset of type-I ELMs is well described by these ideal-MHD (zero resistivity) instabilities in conventional aspect ratio tokamaks [13], where such computations are employed in the EPED model [14, 15] to successfully predict the pedestal structure. A long standing problem has been the application to STs such as the National Spherical Torus Experiment (NSTX), where the predictions of ideal-MHD PB analysis often do not reflect experimental observations, e.g. by finding all edge modes to be stable in ELMy discharges [16–20]. While this prediction is consistent with improved (ideal) stability properties of STs, the reasons for this discrepancy might be associated with the limitation to ideal-MHD computations in the existing models. Most studies of peeling-ballooning modes (PB modes)—both in conventional and low-aspect ratio—have been carried out using ideal-MHD models [16, 21, 22]. Studies of non-ideal MHD effects on PB modes have been

* Author to whom any correspondence should be addressed.

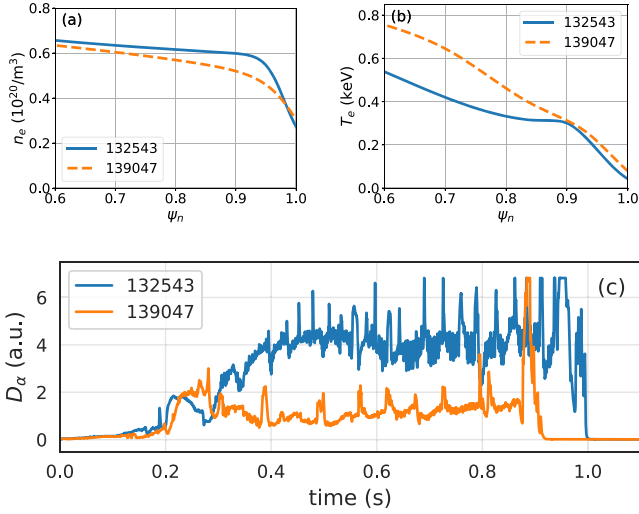


Figure 1. Reconstructed profiles of (a) electron density n_e and (b) electron temperature T_e as a function of the normalized poloidal flux ψ_N prior to the onset of ELMs. The pedestal top is located around $\psi_N = 0.9$. (c) Divertor D_α emission time trace. Spikes indicate the onset of ELMs.

carried out for simple toroidal configurations [23] where low-aspect ratio, shaping and the presence of an X-point were not taken into account. Other numerical work indicates that non-ideal effects can affect PB stability under certain conditions in JET-ILW discharges [24], but does not identify which of these effects are important, nor its applicability to STs.

Resistive ballooning modes have been described analytically in simple geometries [25], where it was found that the inclusion of resistivity can expand the unstable region in ballooning space into the first region of (ideal) ballooning stability [26, 27]. Since calculations with existing PB models indicate stability boundaries inconsistent with experiments on NSTX, in this work we investigate the impact of resistivity on PB modes. In this work, we allow for both, non-ideal MHD effects and realistic ST geometry. In this letter, we demonstrate that the inclusion of resistive physics has a destabilizing effect on the PB modes in NSTX discharges, and can have an especially significant effect on the stability threshold of kink-peeling modes. In this model, NSTX discharges are located on the unstable side of the PB stability boundary, consistent with the onset of ELMs in the experiment. We employ the extended-MHD code M3D-C1 [28, 29] for the linear stability simulations, and compare our new findings with the results of linear computations with the ELITE eigenvalue code [11, 12], which is widely employed in computations of edge stability.

In the remainder of this letter we introduce the characteristics of the simulated ELMing NSTX discharges, describe the simulation model, and show the destabilizing effect of resistivity on PB modes.

In our study we consider two typical (often termed ‘narrow pedestal’) H-mode discharges 132543 and 139047 [19], which both exhibit type-I ELMs. The linear stability simulations are based on a kinetic EFIT equilibrium reconstruction [30–32]. Figure 1 shows the reconstructed radial electron density n_e and electron temperature T_e profiles at the edge for both discharges

as well as the time trace of the D_α emission indicating ELM onset. To obtain a better spatial resolution for the n_e and T_e profiles, the measurements of the Thomson scattering diagnostics are averaged during the last 20% of the inter-ELM period [33], in time windows of 74 ms around 700 ms for discharge 132543 and 30 ms around 665 ms for discharge 139047, respectively. Each interval contains two Thomson profile measurements. The equilibria are reconstructed from experimental measurements up to the last closed flux surface. In order to avoid discontinuities at the plasma edge, we smoothly extend the plasma profiles into the open field line region by fitting a function of the form $c_1[1 - \tanh(c_2(\psi_N - c_3))]$ to the electron density n_e and electron temperature T_e profiles, where ψ_N is the normalized poloidal flux and c_1, c_2 and c_3 are free parameters. Plasma resistivity η is assumed to follow Spitzer’s law [34] and is proportional to $T_e^{-3/2}$. In order to investigate the effect of resistivity on PB modes we consider both the physical (classical) resistivity profiles, and uniformly scaled profiles. In addition to the resistive scaling in M3D-C1 we calculate the growth rate with the ideal-MHD eigenvalue code ELITE via the OMFIT framework [32].

The linear simulations are carried out for toroidal mode numbers from $n = 1$ to 20, which are typically the most relevant for PB modes. We employ the code M3D-C1 [28] to solve the following set of resistive single-fluid MHD equations:

$$\begin{aligned} \frac{\partial \varrho}{\partial t} + \nabla \cdot (\varrho \mathbf{u}) &= 0, \\ \varrho \left(\frac{\partial \mathbf{u}}{\partial t} + \mathbf{u} \cdot \nabla \mathbf{u} \right) &= \mathbf{J} \times \mathbf{B} - \nabla p - \nabla \cdot \Pi, \\ \frac{\partial p}{\partial t} + \mathbf{u} \cdot \nabla p + \Gamma p \nabla \cdot \mathbf{u} &= (\Gamma - 1) [\eta J^2 - \nabla \cdot \mathbf{q} - \Pi : \nabla \mathbf{u}], \\ \mathbf{E} &= -\mathbf{u} \times \mathbf{B} + \eta \mathbf{J}, \\ \mathbf{J} &= \frac{1}{\mu_0} \nabla \times \mathbf{B}, \quad \frac{\partial \mathbf{B}}{\partial t} = -\nabla \times \mathbf{E}, \end{aligned} \quad (1)$$

where, as usual, \mathbf{B} denotes the magnetic field, p the pressure, ϱ the ion mass density, \mathbf{u} the fluid velocity, \mathbf{J} the current density, \mathbf{E} the electric field, η the resistivity, Π the viscous stress tensor and \mathbf{q} the heat flux density [29]. The system of equations (1) is solved in a region that extends beyond the separatrix to the resistive wall. Plasma rotation typically does not have a significant effect on ideal PB stability [35], but this might not necessarily be the case when non-ideal MHD effects are considered [36]. Since PB modes are typically observed to rotate in the direction of the ion fluid, we choose to set the fluid velocity to the measured toroidal ion rotation (we do not modify the equilibrium to take centrifugal effects into account). The linear growth rates determined with M3D-C1 are calculated as $\gamma = \frac{1}{2} d/dt \ln(E_{\text{kin}})$, where E_{kin} is the plasma kinetic energy. In order to map the PB stability boundary, we will vary the pedestal pressure and current density with the Varyped tool [33].

First, we determine the influence of resistivity on the linear growth rate of PB modes based on the equilibrium reconstructions of the two NSTX discharges by scaling the Spitzer resistivity profile η with factors lying in the range of 0.1 to 10. Note

that these factors are chosen to show the resistive scaling and do not necessarily represent the real physical value. We consider $\eta \times 0.1$ as the ideal limit, as the growth rates are almost unaffected by a further decrease of resistivity in the cases presented here. In the following, we normalize the growth rates γ with respect to the Alfvén frequency $\omega_A = B_0 / (L_0 \sqrt{\mu_0 N_0 m_i})$, using $L_0 = 1$ m, $B_0 = 1$ T, $N_0 = 10^{20}$ m⁻³ and m_i being twice the proton mass. Figure 2 shows the normalized linear growth rate γ/ω_A as a function of the toroidal mode number n . While at low values of n the growth rate is independent of resistivity, γ increases with η for modes with $n \gtrsim 5$. An explanation for these two different behaviors can be found by inspection of the eigenfunctions $\xi \propto \delta p = p(t > 0) - p(t = 0)$ in figure 3, which shows ξ in real space and its poloidal Fourier harmonics. The growth rates at low n correspond to ideal core modes that peak around $\psi_N = 0.3$. If low- n PB modes co-exist with these ideal modes their magnitude is small enough to be neglected. Clear edge modes with PB character (cf figure 3) are found at intermediate and large values of n , but as seen in figure 2 their growth rate strongly scales with resistivity. While these resistive edge modes are stable in the case $\eta \times 0.1$, they are unstable at realistic values of resistivity (i.e. Spitzer resistivity) and not much slower than the ideal core mode. As resistivity is increased the resistive edge modes become more unstable and in the case of $\eta \times 10$ even faster than the ideal mode. In a real tokamak discharge the actual resistivity would be somewhat larger than in the $\eta \times 1$ case, both due to neoclassical effects and due to impurities (as η scales with the effective charge Z_{eff}). In the ideal limit, which we consider as 10% of Spitzer resistivity, the PB modes become stable. This result is consistent with the ideal-MHD growth rates calculated with the ELITE code for $n = 5$ –20. The ballooning character of the edge mode eigenfunctions as seen in figure 3 is consistent with experimental findings that confirm an I_p^2 dependence [19], which is typical for ballooning modes.

After demonstrating the existence of PB modes at realistic plasma resistivity, we now determine the stability boundary of PB modes using the M3D-C1 model of equation (1). As in the ideal-MHD stability studies with the ELITE code, we employ the Varyped tool [33] to create a series of equilibria around the experimental kinetic EFIT equilibrium reconstruction, where the edge pressure and current density are varied. In these variations the core profiles are adjusted such that the total stored plasma energy and collisionality remain constant. The so obtained equilibria will provide the initial conditions for the linear stability simulations with M3D-C1, but also for our benchmark with ELITE. The equilibria are parameterized by the flux surface-averaged current density j and the normalized pressure gradient α [37] in the pedestal. In the following we normalize the growth rates with respect to half of the effective diamagnetic frequency in the pedestal $\omega_{*i} \equiv \omega_{*i}^{\text{max}}/2$, where ω_{*i}^{max} is the maximum of the ion diamagnetic frequency in the pedestal region. With this normalization the plasma is considered stable if $\gamma/(\omega_{*i}/2) < 1$ and unstable if $\gamma/(\omega_{*i}/2) > 1$ [15]. (It is this normalization that introduces diamagnetic effects in the ideal-MHD code ELITE.) This allows us to consider diamagnetic effects in the M3D-C1

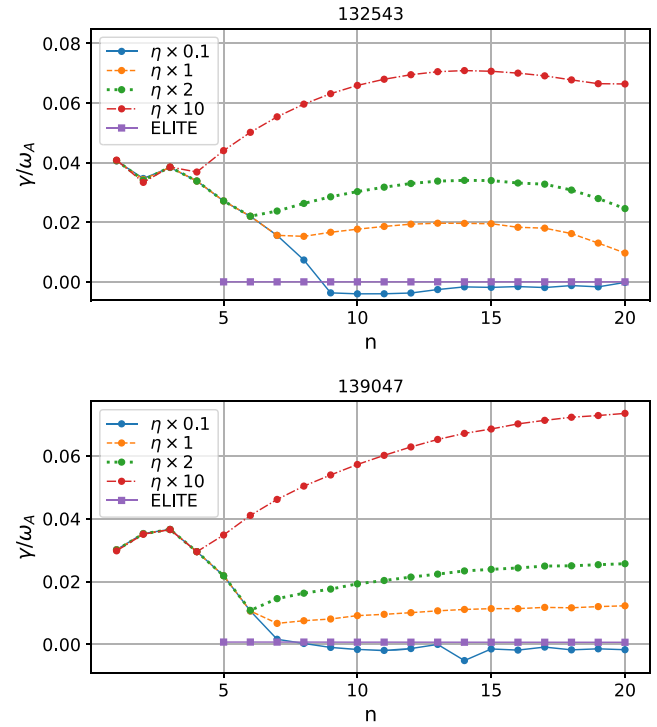


Figure 2. Normalized growth rate γ/ω_A for NSTX discharge 132543 (top) and 139047 (bottom) for various values of the resistivity [$\eta \times 1$ represents the physical (Spitzer) resistivity]. Equilibrium rotation is considered in these simulations. In both shots a clear dependency on resistivity is visible for PB modes.

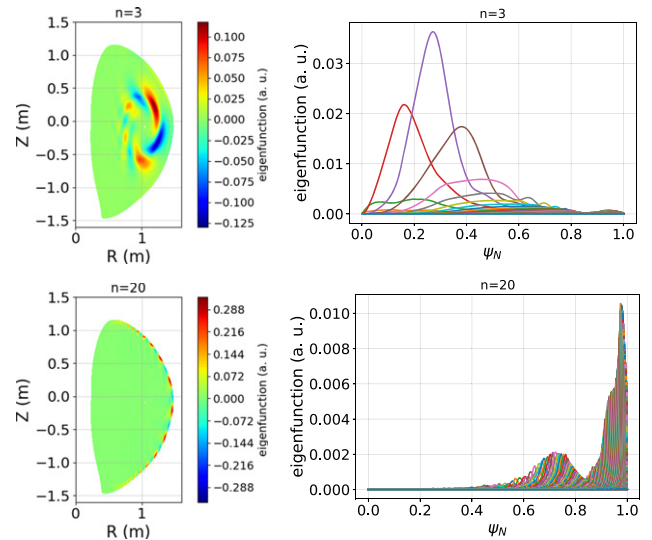


Figure 3. Eigenfunction ξ of the $n = 3$ mode (top) and $n = 20$ mode (bottom) in discharge 132543. (Left) ξ at toroidal angle $\phi = 0$. (Right) Poloidal spectrum showing clear ballooning-like features near the last closed flux surface for $n = 20$.

single-fluid model consistent with ELITE, and thus to provide a meaningful comparison between the two approaches.

Figure 4 shows the effect of plasma resistivity on the stability boundary of PB modes in NSTX discharge 132543 in the inter-ELM phase at 700 ms. The linear growth rates γ are calculated with Spitzer resistivity and in the ideal limit

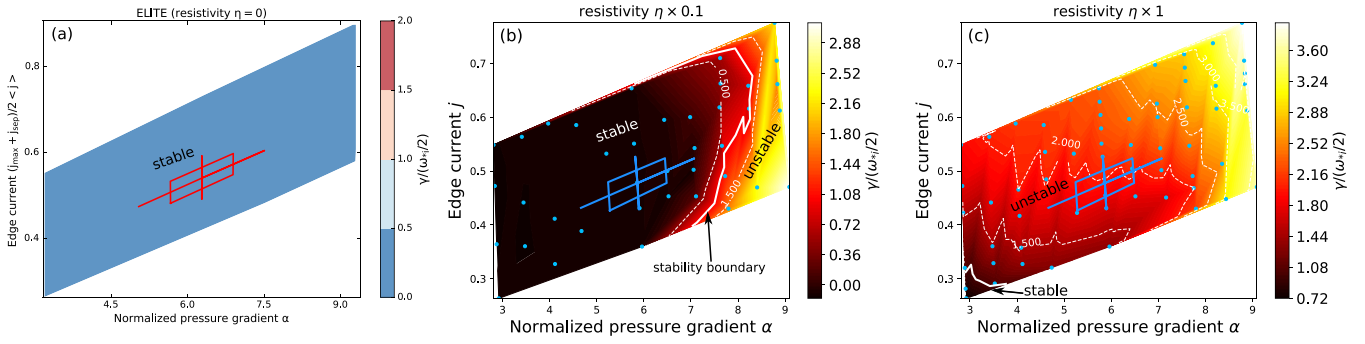


Figure 4. PB stability boundary and normalized growth rate $\gamma/(\omega_{*i}/2)$ of the most unstable mode calculated for equilibrium variations of NSTX discharge 132543 with (a) the ideal-MHD model of ELITE. (b) M3D-C1 in the ideal limit. (c) M3D-C1 using Spitzer resistivity. The bold solid lines represent the stability boundary and the cross shows the location of the discharge.

(Spitzer resistivity multiplied by 0.1) with M3D-C1 and compared with the ideal-MHD growth rates calculated with the ELITE code. At large values of α , i.e. strong edge pressure gradients, the plasma is unstable to PB modes in the ideal limit as well as in the resistive simulations. This constitutes a region of ideal PB mode instability as the growth rate depends only very weakly on resistivity. While in the ideal limit (figure 4(b)) this region is far away from the location of the actual discharge (indicated by a cross in figure 4) in parameter space, the situation is different when realistic plasma resistivity is considered in the model. It can be seen from figure 4(c) that the unstable region is well extended compared with the ideal limit. The region of ideal instability is surrounded by a region where the plasma is unstable, but with lower growth rates than in the ideal region. This can be interpreted as a region where resistivity destabilizes PB modes with moderate edge current density. The transition from the resistive to the ideal region of instability is very steep on the ballooning side (large α), while on the kink side (current limited) it is shallower (cf contour lines in figure 4(c)). This markedly contrasts with ideal-MHD results, in which the kink-peeling (current-driven) stability threshold is very steep [38]. The most unstable modes on the ballooning side have toroidal mode number $n = 20$, whereas on the peeling side the toroidal mode number of the most unstable mode is lower, ranging from $n = 11$ –20. This behavior is expected, but the mode numbers on the peeling side are slightly higher than what is observed in conventional aspect ratio machines [13]. While the experimental point is deep inside the unstable domain in the resistive calculation, more refined models including (stabilizing) finite Larmor radius effects [23, 39, 40] might show a stability boundary closer to the experimental point, thus explaining why it is experimentally accessible. Neoclassical corrections to Spitzer resistivity are expected to provide similar results with slightly larger growth rates, whereas finite Larmor radius effects are seen to be stabilizing in M3D-C1 simulations. These refined models are subject to future publication. In the ideal limit M3D-C1 and ELITE consistently show that NSTX discharge 132543 is located in the region where PB modes are stable and thus should not exhibit ELMs. However, when Spitzer resistivity is considered, the discharge lies on the unstable side within the region of resistive instability. While the ELITE

results are reasonably well converged in most of the domain it is possible with certain parameter to obtain instability for large values of α and j [41]. This does not affect the interpretation that the discharge is located inside the stable domain.

We now benchmark our model with previously established ELITE results from DIII-D discharge 147105 at 3750 ms [38], a point where the plasma exhibits type-I ELMs. In this context we demonstrate that unlike in low-aspect ratio resistivity affects the stability boundary only weakly in large aspect ratio discharges. The stability boundary calculated with these different models is shown in figure 5. Consistent with the observation of ELMs in the experiment the ideal-MHD ELITE model predicts that the discharge is located in the unstable domain. This result is recovered with the M3D-C1 simulations in which the resistivity has been reduced below the Spitzer value by a factor of 10 in order to approach the ideal limit. The stability boundary is shifted slightly towards larger values of α and j . In previous linear simulations of simplified equilibria M3D-C1 has shown very good agreement with ELITE [42], when the initial conditions in M3D-C1 are adjusted to match those of ELITE. However, the presented cases are based on reconstructions of diverted experimental equilibria and for such configurations weak differences between ELITE and M3D-C1 are expected, even in the limit where the plasma resistivity goes to zero in M3D-C1. Due to the coordinate singularity arising from the x -point in a diverted configuration, ELITE places the plasma-vacuum interface slightly inside the separatrix. In contrast, in M3D-C1 the separatrix and private flux region are included in the computational domain and the density and temperature profiles vary smoothly across the separatrix. While the cutoff close to the separatrix results in slightly lower growth rates in ELITE, M3D-C1 simulates the presence of the vessel wall and uses nonuniform density and temperature profiles, which in turn have stabilizing effects on the plasma. For more details we refer to reference [42]. Now, when a more physically realistic resistivity is considered the stability boundary remains almost unaffected as seen in figure 5(c). These results indicate—together with the successful application of ELITE to a number of conventional aspect-ratio tokamaks—that in large aspect ratio discharges the stability boundary is almost unaffected by resistivity, thus justifying the use

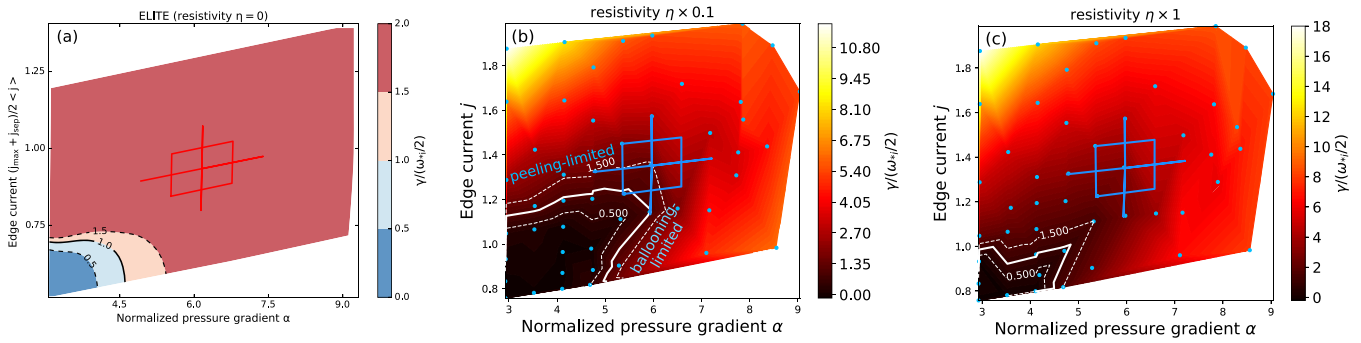


Figure 5. PB stability boundary of DIII-D discharge 147105 calculated with (a) ELITE. (b) M3D-C1 in the ideal limit. (c) M3D-C1 using Spitzer resistivity. The bold solid lines represent the stability boundary and the cross shows the location of the discharge. In all models the discharge is consistently located on the unstable side. Note that the axis limits do not extend to $\alpha = j = 0$, the origin of the stable region.

of ideal-MHD, while in low-aspect ratio NSTX discharges a resistive PB stability boundary is met well before the ideal stability boundary is reached.

In summary, we have shown for the first time that plasma resistivity can have a significant effect on the PB stability threshold, especially for current-driven modes (modes at the peeling-side of parameter space) in ST configurations. When a resistive single-fluid MHD model is considered the stability boundary shifts to much lower values of pedestal pressure gradient and current density relative to ideal-MHD models, and correctly locates ELMy discharges on the unstable side. This model can be applied in future studies to determine the stability boundaries in various operation scenarios in STs. Our results suggest that the inclusion of plasma resistivity can provide an explanation for the onset of ELMs in STs and is crucial in the modeling of PB modes in these machines, while ideal-MHD models are sufficient for conventional aspect ratio machines. This finding constitutes a basis for the development of a pedestal model to allow the prediction of ELMs in NSTX and other STs, i.e. an EPED-like model that calculates the limiting pedestal width and height in STs.

Acknowledgments

The authors thank Orso Meneghini, Sterling Smith and Phil Snyder for useful discussions. This research used resources of the National Energy Research Scientific Computing Center, which is supported by the Office of Science of the US Department of Energy under Contract No. DE-AC02-05CH11231. This work was supported by the US Department of Energy under Contracts DE-AC02-09CH11466, DE-FC02-04ER54698 and the Department of Energy early career research program. The United States Government retains a non-exclusive, paid-up, irrevocable, world-wide license to publish or reproduce the published form of this manuscript, or allow others to do so, for United States Government purposes.

ORCID iDs

A. Kleiner <https://orcid.org/0000-0002-5800-8027>

A. Diallo <https://orcid.org/0000-0002-0706-060X>

References

- [1] Peng Y.-K.M. and Strickler D.J. 1986 *Nucl. Fusion* **26** 769
- [2] Canik J.M. et al 2013 *Nucl. Fusion* **53** 113016
- [3] Peeters A.G. 2000 *Plasma Phys. Control. Fusion* **42** B231
- [4] Strait E.J. 1994 *Phys. Plasmas* **1** 1415
- [5] Sykes A. 1999 *Tech. Phys.* **44** 1047
- [6] Ono M. and Kaita R. 2015 *Phys. Plasmas* **22** 040501
- [7] Wagner F. et al 1982 *Phys. Rev. Lett.* **49** 1408
- [8] Zohm H. 1996 *Plasma Phys. Control. Fusion* **38** 105
- [9] Federici G., Loarte A. and Strohmayer G. 2003 *Plasma Phys. Control. Fusion* **45** 1523
- [10] Wilson H.R., Cowley S.C., Kirk A. and Snyder P.B. 2006 *Plasma Phys. Control. Fusion* **48** A71
- [11] Snyder P.B. et al 2002 *Phys. Plasmas* **9** 2037
- [12] Wilson H.R., Snyder P.B., Huysmans G.T.A. and Miller R.L. 2002 *Phys. Plasmas* **9** 1277
- [13] Burrell K.H., Osborne T.H., Snyder P.B., West W.P., Fenstermacher M.E., Groebner R.J., Gohil P., Leonard A.W. and Solomon W.M. 2009 *Nucl. Fusion* **49** 085024
- [14] Snyder P.B., Groebner R.J., Leonard A.W., Osborne T.H. and Wilson H.R. 2009 *Phys. Plasmas* **16** 056118
- [15] Snyder P.B., Groebner R.J., Hughes J.W., Osborne T.H., Beurskens M., Leonard A.W., Wilson H.R. and Xu X.Q. 2011 *Nucl. Fusion* **51** 103016
- [16] Maingi R. et al (The NSTX Research Team) 2009 *Phys. Rev. Lett.* **103** 075001
- [17] Boyle D.P. et al 2011 *Plasma Phys. Control. Fusion* **53** 105011
- [18] LeBlanc A.C. et al 2011 *Nucl. Fusion* **51** 103022
- [19] Diallo A. et al 2011 *Nucl. Fusion* **51** 103031
- [20] Diallo A. et al 2013 *Nucl. Fusion* **53** 093026
- [21] Groebner R.J. et al 2013 *Nucl. Fusion* **53** 093024
- [22] Medvedev S.Y., Martynov A.A., Martin Y.R., Sauter O. and Villard L. 2006 *Plasma Phys. Control. Fusion* **48** 927
- [23] Xia T.Y., Xu X.Q. and Xi P.W. 2013 *Nucl. Fusion* **53** 073009
- [24] Pamela S.J.P. et al 2017 *Nucl. Fusion* **57** 076006
- [25] Conner J.W., Hastie R.J. and Martin T.J. 1985 *Plasma Phys. Control. Fusion* **27** 1509
- [26] Strauss H.R. 1981 *Phys. Fluids* **24** 2004
- [27] Sykes A., Bishop C.M. and Hastie R.J. 1987 *Plasma Phys. Control. Fusion* **29** 719
- [28] Jardin S.C. 2004 *J. Comput. Phys.* **200** 133
- [29] Breslau J., Ferraro N. and Jardin S. 2009 *Phys. Plasmas* **16** 092503
- [30] Lao L.L., John H.S., Stambaugh R.D., Kellman A.G. and Pfeiffer W. 1985 *Nucl. Fusion* **25** 1611
- [31] Lao L.L. et al 2005 *Fusion Sci. Technol.* **48** 968
- [32] Meneghini O. et al 2015 *Nucl. Fusion* **55** 083008
- [33] Osborne T.H. et al 2008 *J. Phys.: Conf. Ser.* **123** 012014

- [34] Cohen R.S., Spitzer L. and Routly P.M. 1950 *Phys. Rev.* **80** 230
- [35] Snyder P.B. *et al* 2007 *Nucl. Fusion* **47** 961
- [36] Xi P.W., Xu X.Q., Wang X.G. and Xia T.Y. 2012 *Phys. Plasmas* **19** 092503
- [37] Miller R.L., Chu M.S., Greene J.M., Lin-Liu Y.R. and Waltz R.E. 1998 *Phys. Plasmas* **5** 973
- [38] Wade M.R. *et al* 2015 *Nucl. Fusion* **55** 023002
- [39] Roberts K.V. and Taylor J.B. 1962 *Phys. Rev. Lett.* **8** 197
- [40] Cooper W.A. 1982 *Plasma Phys.* **24** 265
- [41] Snyder P.B. 2020 personal communication
- [42] Ferraro N.M., Jardin S.C. and Snyder P.B. 2010 *Phys. Plasmas* **17** 102508